

Self-organized mode-locking effect in superconductor/ferromagnet hybrids

J. Van de Vondel,¹ A. V. Silhanek,¹ V. Metlushko,² P. Vavassori,^{3,4} B. Ilic,⁵ and V. V. Moshchalkov¹

¹*Nanoscale Superconductivity and Magnetism Group, INPAC-Institute for Nanoscale Physics and Chemistry, K. U. Leuven, Celestijnenlaan 200D, B-3001 Leuven, Belgium*

²*Department of Electrical and Computer Engineering, University of Illinois, Chicago, Illinois 60607, USA*

³*Department of Physics, INFN-National Research Center on nanoStructures and Biosystems at Surfaces (S3), University of Ferrara, via Saragat 1, I-44100 Ferrara, Italy*

⁴*CIC nanoGUNE Consolider, Tolosa Hiribidea 76, 20018 Donostia-San Sebastian, Spain*

⁵*Cornell Nanofabrication Facility, School of Applied and Engineering Physics, Cornell University, Ithaca, New York 14853, USA*

(Received 1 October 2008; revised manuscript received 3 February 2009; published 27 February 2009)

The vortex dynamics in a low-temperature superconductor deposited on top of a rectangular array of micrometer size permalloy triangles is investigated experimentally. The rectangular unit cell is such that neighboring triangles physically touch each other along one direction. This design stabilizes remanent states which differ from the magnetic vortex state typical of individual noninteracting triangles. Magnetic force microscopy images have revealed that the magnetic landscape of the template can be switched to an ordered configuration after magnetizing the sample with an in-plane field. The ordered phase exhibits a broad flux-flow regime with relatively low critical current and a highly anisotropic response. This behavior is caused by the spontaneous formation of two separated rows of vortices and antivortices along each line of connected triangles. The existence of a clear flux-flow regime at zero external field supports this interpretation. The density of induced vortex-antivortex pairs is directly obtained using a high-frequency measurement technique which allows us to resolve the discrete motion of vortices. Strikingly, the presence of vortex-antivortex rows gives rise to a self-organized synchronized motion of vortices which manifests itself as field independent Shapiro steps in the current-voltage characteristics.

DOI: [10.1103/PhysRevB.79.054527](https://doi.org/10.1103/PhysRevB.79.054527)

PACS number(s): 74.78.Fk, 74.78.Na, 74.25.Dw, 74.25.Op

I. INTRODUCTION

The dynamics and pinning of vortices in type-II superconductors is arguably one of the most widely investigated phenomena in the field of superconductivity. Recently, particular attention has been devoted to the possibility of controlling the strength of the vortex pinning using different magnetic templates.^{1,2} Within the London formalism, the interaction between a vortex line and a finite-size permanent magnet is given by³

$$U_p(\mathbf{R}) = - \int_{\text{dot}} \mathbf{m} \cdot \mathbf{B}_v(\mathbf{R} - \mathbf{r}) d^3r, \quad (1)$$

where the integration is carried out over the volume of the ferromagnet, \mathbf{R} indicates the position of the vortex line, \mathbf{m} is the magnetic moment of the ferromagnetic dot and \mathbf{B}_v is the field generated by the vortex line. Strictly speaking, Eq. (1) is valid within the point magnetic-dipole approximation or for a ferromagnetic dot with homogeneous magnetization.³ This equation shows that the pinning potential not only depends on the size of the dots^{2,4} but also on their exact magnetic state.⁵ In particular, if the superconducting penetration depth λ is on the order of the lateral size of the dot, a weak average pinning is expected when the magnetic dot contains multiple domains. In contrast to that, a maximum pinning should be achieved for single domain structures. In order to retain these properties in big arrays of magnetic particles it is necessary to ensure a minimum distance between them in such a way that the field profiles of neighboring elements do not overlap and can be resolved at scales of the magnetic penetration length λ .

According to Eq. (1), it is possible to increase the pinning potential by just growing continuously the magnetic moment of the dots. This growth is limited by the fact that above certain magnetic moment, a vortex-antivortex (v-av) pair will be induced by the magnetic element with the consequent change in the pinning properties.⁶ For instance, dots with perpendicular magnetic moment induce a vortex on top of the dots whereas the accompanying antivortex is located at interstitial positions, in between the dots. As a result, vortices and antivortices feel a different pinning potential which leads to a distinct dynamic response.⁷ The weakly pinned interstitial antivortices limit the maximum critical current, J_c^{max} , and therefore their annihilation with an external field produces a shift of the field position of the J_c^{max} toward $H = nH_1$, where n is the number of vortex-antivortex pairs generated by a single magnetic element and H_1 is the field corresponding to one external vortex per unit cell. Since H_1 is a geometrically predefined parameter, the field loci of the J_c^{max} is a direct measurement of the number n of bounded pairs. Unfortunately, in the case of micromagnets with in-plane magnetic moment, the field polarity symmetry of the system conceals this information from dc electro-transport experiments.

In this work, we discuss alternative methods to accurately determine the number n of vortex-antivortex pairs induced by the magnetic template, based on the ac-dynamic response of the hybrid system. Indeed, the fact that the critical force to bring the vortex and antivortex closer differs from that necessary to pull them apart,⁸ gives rise to a clear rectification effect when the system is submitted to a zero average ac signal. This rectified voltage is maximum at zero external field⁹ and progressively decreases with increasing field until

all vortices (or antivortices) are compensated. At rf frequencies the mode locking or synchronized motion of vortices produces distinct voltage steps in the current-voltage characteristics with separation determined by the number of moving vortices. Both techniques indicate that for the particular system here investigated, the magnetic template generates one single vortex-antivortex pair per unit cell.

The crucial conditions for the success of these methods are (i) a periodic landscape, i.e., all vortices and antivortices feeling the same environment, and (ii) a free flux-flow motion of vortices. Although the predefined topological landscape is by definition periodic, the magnetic landscape for the as-grown state consists of a highly disorder distribution of magnetic poles. This disordered state can be switched to a perfectly ordered magnetic lattice by magnetizing the sample with an in-plane field. The order-disorder transition, already reported for other *S/F* systems,¹⁰ produces a profound modification in the vortex dynamics. More specifically, in the disordered state, nonlinear current-voltage characteristics with high critical currents are observed, whereas a very broad flux-flow regime accompanied by a sharp decrease in the critical currents is obtained in the ordered state. This behavior can be attributed to the reduction of the average hopping distance determined by the separation between neighboring magnetic poles of identical polarity. In addition, the presence of a flux-flow regime at zero applied field reinforces the idea that the investigated magnetic structure is able to induce vortex-antivortex pairs.

II. SAMPLE PREPARATION AND CHARACTERIZATION

The sample investigated consists of a periodic array of permalloy ($\text{Ni}_{80}\text{Fe}_{20}$) equilateral triangles of $1\ \mu\text{m}$ side and a thickness of 25 nm. Along one of the principal directions of the array (x axis) the separation between the triangles is $1\ \mu\text{m}$ (period in the x direction is $2\ \mu\text{m}$) whereas in the perpendicular direction (y axis) the triangles are touching [see Fig. 1(a)], which results in a period of $0.866\ \mu\text{m}$ in the y direction. The surface of the unit cell is $S=1.732\ \mu\text{m}^2$, giving a value of 1.193 mT for the first matching field, $H_1 = \phi_0/S$ (here $\phi_0 = h/2e$ is the flux quantum).

This geometry gives rise to two well defined directions of the structure, parallel (y) and perpendicular (x) to the line connecting nearby triangles, as indicated in Fig. 1(a). A 50 nm thick superconducting Al bridge (width= $100\ \mu\text{m}$) deposited on top of the magnetic template also covers the unpatterned substrate [see Fig. 1(b)] thus allowing us to compare directly patterned vs reference plain film and identify the influence of the magnetic triangles on the superconductor. A 10 nm thick Si layer electrically separates the Al bridge from the magnetic template in order to avoid proximity effects. Both the array of triangles and the transport bridge are aligned at submicrometer scale and were prepared by standard lithographic techniques. The Al plain film has a critical temperature at zero field $T_{c0}=1.315\ \text{K}$, with residual resistivity ratio $R(300\ \text{K})/R(4.2\ \text{K}) \sim 2$, and superconducting coherence length $\xi(0) \approx 128\ \text{nm}$.

The fact that neighboring triangles overlap in one direction allows us to achieve two well distinguished phases: dis-

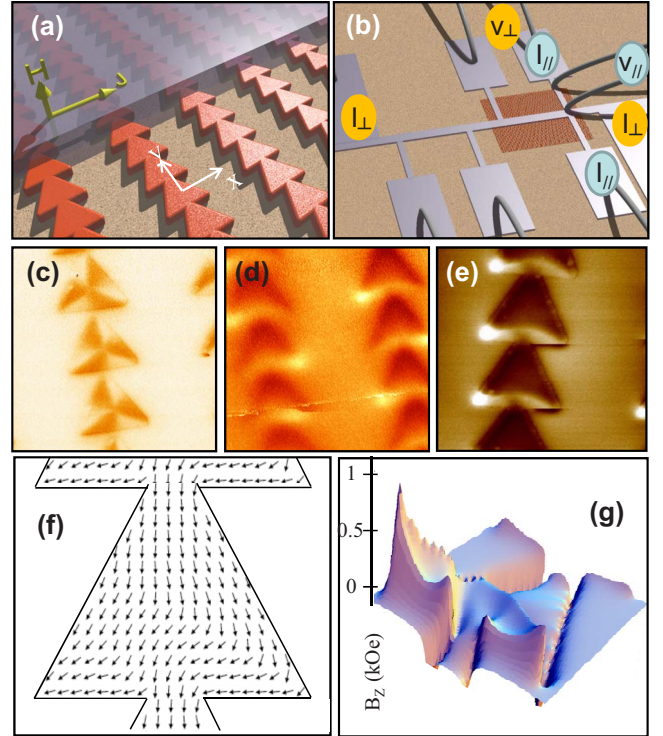


FIG. 1. (Color online) (a) Schematic of the array of Py triangles. The direction of the external field, the relative orientation of the array, and the current perpendicular to the chain of triangles is clearly indicated with arrows. (b) Schematic of the Al transport bridge partially covering the magnetic pattern (shaded region). The current and voltage contacts are shown for transport measurements with a current applied parallel ($I_{\parallel}, V_{\parallel}$) and perpendicular (I_{\perp}, V_{\perp}) to the chain of triangles. Magnetic force microscopy pictures obtained at remanence of physically separated magnetic triangles (c), touching magnetic triangles in the virgin state (d), and the triangles magnetized perpendicular to the chain of triangles (e). Panels (f) and (g) show the local magnetic-moment distribution and the z component of the stray field (B_z), respectively, calculated by OOMMF simulations (Ref. 14).

ordered in the as-grown state and ordered in the magnetized state. Indeed, magnetic force microscopy (MFM) images shown in Fig. 1(c) for nontouching triangles demonstrate that the remanent state, irrespective of the magnetic history of the triangles, is always a vortex state, in agreement with previous reports on individual micrometer size magnetic structures.^{11,12} In contrast to that, if there is physical contact between neighboring triangles a new set of possible states can be found. Figure 1(d) shows a MFM image of the sample investigated in the as-grown state. Here a clearly disordered arrangement of the, so-called, buckle states¹³ is observed. Interestingly, after magnetizing the sample with a homogeneous in-plane field perpendicular to the chain of triangles [Fig. 1(e)], these buckle states can be set in a perfectly ordered arrangement. The in-plane distribution of magnetic moments calculated by object oriented macromagnetic framework (OOMMF) micromagnetic simulations¹⁴ is indicated in Fig. 1(f) with black arrows whereas the z component of the stray field (B_z) is shown in Fig. 1(g). In all cases the magnetic state of each triangle is characterized by a strong

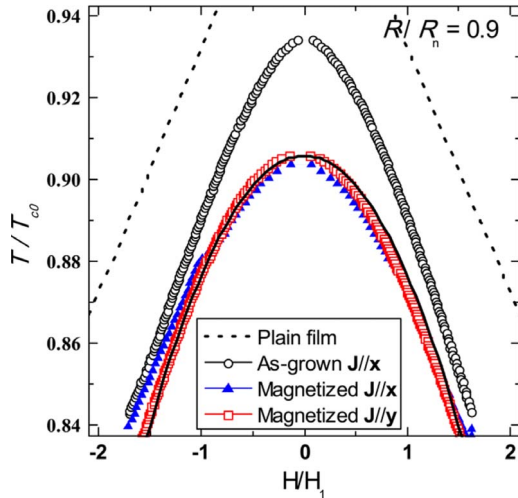


FIG. 2. (Color online) Superconducting-normal phase boundary as determined by 90% resistance criterion of the normal resistance R_n and dc of 100 μA for the as-grown state (open circles) and the magnetized state for different current orientations. The dashed line shows the corresponding transition lines for the coevaporated Al plain film. The solid line is a fit assuming a lateral confinement of the superconducting condensate (see text).

out-of-plane magnetic pole which is located at one of the two bottom corners of the Py triangles and a weaker magnetic pole, with opposite polarity, located at the top corner of the triangle [Fig. 1(e)]. It is precisely this magnetic pole which can be controlled to lie on either side of the triangle by simply changing the direction of magnetization. Notice that this magnetic monopolelike structure breaks the field polarity symmetry of the S/F hybrid system. The question now arises as whether the distribution of the magnetic dipoles (ordered versus disordered) has any effect on the properties of the adjacent superconducting film.

III. NUCLEATION OF SUPERCONDUCTIVITY

Let us first analyze the nucleation of the superconducting order parameter for the two different magnetic states of the hybrid system. Figure 2 summarizes the obtained superconductor-normal metal phase boundaries for a dc of 100 μA and using 90% criterion of the normal-state resistance R_n for different magnetic states and current orientations.¹⁵ For the as-grown state (open circles) a pronounced decrease in the critical temperature at low fields with respect to the plain film is observed. A further suppression of T_c is obtained after the sample has been magnetized with an in-plane field parallel to the x direction (solid triangles). The fact that the phase boundary of the as-grown state lies in between those corresponding to the plain film and the magnetized state, suggests that in the virgin sample, randomly oriented buckle states coexist with magnetic vortex states. This has been indeed confirmed by the MFM images taken at different locations of the pattern.

It is worth noticing that for the magnetized sample the $T_c(H)$ boundary exhibits a parabolic background similar to that reported in earlier investigations.^{16–18} This behavior can

be ascribed to the change in dimensionality when $\xi(T)$ exceeds the size w of the regions where superconductivity first nucleates. Within this regime the phase boundary can be approximated by $T_c(H)/T_c(0) = 1 - (\alpha H)^2$, with $\alpha = \xi(0)\pi w / \sqrt{3}\phi_0$. By using this expression to fit the data in Fig. 2 (solid line) we found $w \sim 1.4 \mu\text{m}$ which is consistent with the largest separation between neighboring magnetic poles. This behavior suggests that for the magnetized sample the stray fields confine the superconducting condensate in between the magnetic poles and consequently the superconducting order parameter will be modulated into a sequence of quasi-one-dimensional stripes. This prediction is in agreement with complementary transport measurements for two orthogonal orientations of the applied current, perpendicular to the chain of triangles (solid triangular symbols) and parallel to them (open square symbols) as shown in Fig. 2, indicating that the onset of superconductivity is independent on the direction of the applied current.

IV. VORTEX DYNAMICS IN THE ORDERED AND DISORDERED PHASES

In Sec. III we showed that by switching from the as-grown (disordered phase) to the magnetized (ordered phase) state, the number of magnetic poles increases, which in turn gives rise to a decrease in T_c . In this particular case it is the difference in the average field intensity which induces the decrease in T_c .

According to Eq. (1) the vortex dynamics in a magnetic pinning landscape is not only determined by the field intensity but it is also highly sensitive to the polarity of the magnetic field. Therefore deeper in the superconductive state, where the electric response is dominated by the vortex dynamics, a very strong dependence on the distribution of magnetic poles should become apparent.

In order to address this issue we have measured the voltage-current characteristics $[V(I)]$ with the bias current applied in the x direction at $H = \frac{1}{2}H_1$ and $T = 1.1 \text{ K}$ (Ref. 19) for the two different magnetic states: as-grown (open circles) and magnetized (solid squares) states as shown in Fig. 3(a). The most obvious feature in this figure is the enormous difference (more than an order of magnitude) between the critical current of the magnetized state (24 μA) with respect to the demagnetized state (490 μA). Furthermore, the vortex dynamics is severely modified after magnetizing the sample. Indeed, whereas in the as-grown state there is a narrow window of currents exhibiting a highly nonlinear $V(I)$ dependence, where the vortex lattice transit from pinned phase to the normal state, in the magnetized sample a broad flux-flow regime is observed immediately above the critical current. Figures 3(b) and 3(c) summarize the field dependence of the different dynamical phases for the as-grown sample [panel (b)] and after magnetization [panel (c)]. The onset of vortex motion is delimited by a resistance criterion of 10% R_n while a 90% R_n criterion is used to indicate the transition to the normal state.

Notice that the presence of matching features exactly at H_1 , together with the fact that in the magnetized state a finite critical current is needed to depin the vortices, rule out the

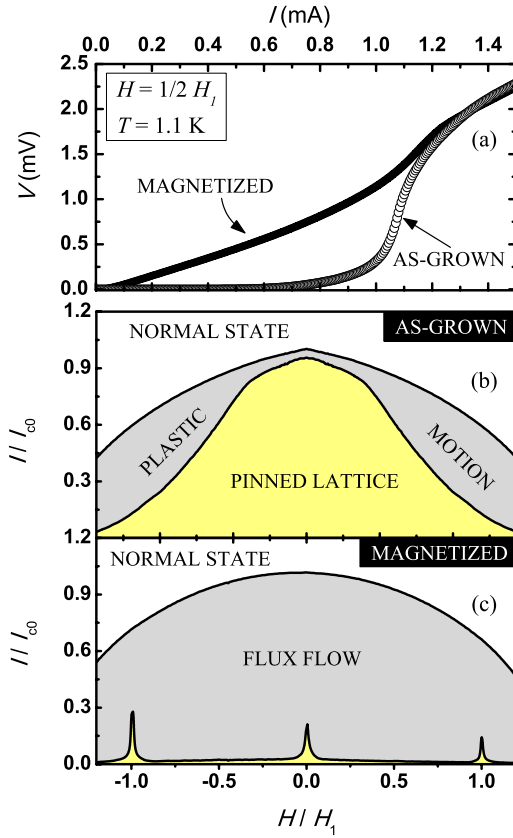


FIG. 3. (Color online) (a) Voltage-current $V(I)$ characteristic with current applied in the x direction, at $H = \frac{1}{2}H_1$ and a temperature of 1.1 K for the as-grown and the magnetized states. The lower panels show the magnetic field dependence of the critical current and the transition to the normal state as determined by criterion of 10% R_n and 90% R_n , respectively, for the (b) as-grown and (c) magnetized states. In both graphs the vertical axis is normalized by I_{c0} , the current needed to transit the demagnetized sample to the normal state at zero applied field.

possibility of having normal-metal stripes in the hybrid sample.²⁰ Instead, the observed difference between both phases can be attributed to the formation of easily moving channels of vortices and antivortices created by the magnetic structure. Indeed, in the ordered phase the potential wells created by the magnetic dipoles are perfectly aligned and strongly overlap, thus creating an easy channel for flux motion. In contrast to that, in the disordered phase, the average distance between two neighboring magnetic pinning centers of equal polarity is larger thus impeding the easy motion of vortices. From now on we will focus on the dynamic response of the system in the ordered state.

V. EVIDENCE OF INDUCED v-av PAIRS

A rough criterion to determine whether the stray field emanating from the magnetic structure is strong enough to induce v-av pairs can be obtained by comparing it to the penetration field H_p resulting from Bean-Livingston barriers.^{21,22} The highest barrier possible is limited by the thermodynamic critical field $H_p = \Phi_0 / (2\sqrt{2}\pi\lambda\xi)$. Using ξ

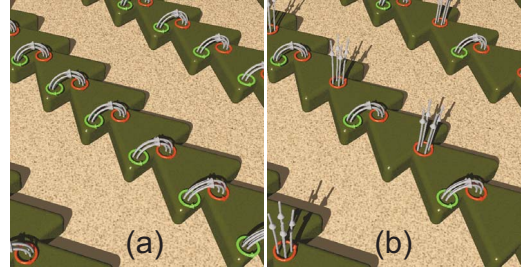


FIG. 4. (Color online) Schematic of the induced vortex lattice (for simplicity we assume only one vortex-antivortex pair generated per unit cell) in the case of no external applied field (a) and an applied field equal to $\frac{1}{2}H_1$ (b).

$= 128$ nm and $\lambda = 150$ nm we obtain $H_p \sim 12$ mT which lies well below the field intensity (~ 100 mT) produced by the magnetic template at the superconducting film. Based on this estimation we can safely conclude that the magnetic structure is able to induce, at least, one vortex-antivortex per unit cell.

This finding suggests that the ordered phase consists of two well defined channels with opposite vortex polarity as schematically shown in Fig. 4(a). For simplicity we assume only one-vortex-antivortex pair.

Since the magnetic template breaks the field polarity symmetry, in principle vortices and antivortices should experience a different depinning current. Moreover, as illustrated in Fig. 4(b), by applying an external field, vortices in the channel with opposite polarity will be annihilated, which will lead to a reduction in the vortex mobility in these rows. On the one hand, the similarity between the partially compensated rows with the as-grown (disordered) state, which corresponds to the highest critical current, indicates that the partially compensated rows should also exhibit a high critical current. On the other hand, it is clear that at every place where a vortex (or antivortex) is annihilated an energetically convenient place for vortices to hop is removed. Since the superconducting order parameter is no longer suppressed in that position, a reduction in the overall mobility of vortices in that particular row is expected. In the extreme situation that a whole line is compensated we should approach to the behavior of the plain film at zero field, which indeed exhibits a high critical current.

In contrast to that, the row with vortices of opposite polarity would remain unaltered. This scenario predicts two anomalous behaviors: the existence of a flux-flow response at zero field and a field independent flux-flow regime as long as none of the two rows of vortices is fully compensated by the external field. Both predictions are in agreement with the field evolution of the $V(I)$ measurements done at 1.1 K. The slope of the linear regime, proportional to the amount of particles contributing to the easy flow, is plotted as a function of field in Fig. 5(a). In comparison to the slope expected for the free flux-flow model $R_{ff} = R_n H / H_{c2}$ [straight line in Fig. 5(a)], where R_n is the normal-state resistance and H_{c2} is the upper critical field, a weak-field dependence of the flux-flow slope is seen at low-field values.

Further evidence in favor of the existence of channels populated with v-av pairs comes from the measurements of

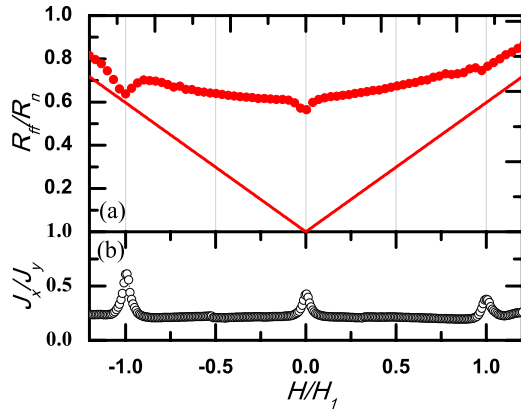


FIG. 5. (Color online) (a) The field dependence of the flux-flow resistance for the magnetized sample at $T=1.1$ K. The straight lines indicate the expected dependence according to free flux-flow model. (b) Critical current as a function of magnetic field at a temperature of 1.1 K for both current directions. A clear anisotropic response is observed.

the critical current for currents applied parallel (J_y) and perpendicular (J_x) to the channels of v-av pairs. These results are shown in Fig. 5(b), with a critical current determined using a criterion of $100 \mu\text{V}$. This figure shows a strong in-plane anisotropy $\gamma=J_x/J_y$ induced by the magnetic template which results from the easier motion of vortices along the line of magnetic poles than perpendicular to them. This anisotropy amounts to a factor of 5 at nonmatching fields and is minimum at the commensurability fields. This anisotropic response is clearly observed independently of the chosen voltage criteria.

VI. DETERMINATION OF THE v-av PAIRS DENSITY AT LOW FREQUENCIES: RATCHETS

The scenario described in Sec. V where rows of vortices and antivortices generated by the magnetic template coexist, makes our system similar to the array of elongated magnetic bars studied by de Souza Silva *et al.*⁹ This system has been modeled within the London approximation by Carneiro⁸ for the case where no v-av pairs are induced, and more recently by Lima and de Souza Silva²³ assuming that v-av pairs emanate from the dipoles. Irrespective of whether the magnetic template is able to induce v-av pairs or not, both situations lead to a rectification of the net vortex motion v when a zero average ac force is applied parallel to the dipolar moment (i.e., along the line connecting a vortex with its corresponding antivortex).²⁴ However, clear differences in the field dependence of the average velocity are expected. Indeed, if v-av pairs are present then (i) a maximum rectification is expected at zero field, (ii) unlike standard ratchet signal, the sign of the average voltage readout should be field polarity independent, (iii) as vortices (antivortices) are progressively compensated by increasing the external negative (positive) field, the rectified signal should decrease.

The measured rectification effect, shown in Fig. 6, confirms all the above mentioned facts and indicates that the v-av pairs are more easily brought together than separated.

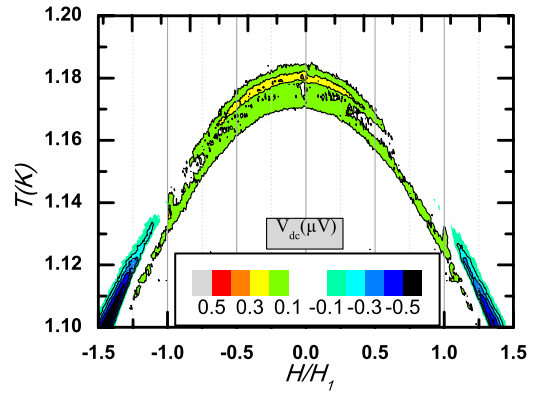


FIG. 6. (Color online) Rectified voltage V_{dc} in the temperature-field (T - H) plane for the magnetized sample subjected to a 1 kHz sinusoidal ac in the y direction of amplitude $100 \mu\text{A}$.

Furthermore, if the applied field is increased above the first matching field a sign reversal occurs. This sign reversal at H_1 cannot be explained assuming more than one v-av pair created by the magnetic template since in this case the v-av annihilation process would be unlikely interrupted by the partial compensation of one row of vortices. In contrast to that, if there is a single v-av pair per unit cell, once a whole line is compensated by the external field, a dramatic change in the rectification properties is expected. Although this finding seems to indicate that the magnetic structure is able to induce a single v-av per triangular element, a more convincing evidence of this prediction can be obtained only by monitoring the coherent motion of vortices at higher frequencies.

VII. DETERMINATION OF THE v-av PAIRS DENSITY AT HIGH FREQUENCIES: MODE LOCKING

The motion of vortices in a periodic potential gives rise to a variety of interesting dynamical effects such as the generation of rf radiation²⁵ and synchronization-resonance effects of the vortex lattice^{26–28} when a rf current I_{rf} is superimposed onto a dc drive I_{dc} . The latter effect gives rise to a series of plateaus in the $V(I)$ measurements very similar to the Shapiro steps observed in Josephson junctions.²⁹ The relevant time scale of these processes is determined by the washboard frequency, $f=v/d$ with d the period of the potential, and v the average velocity of the particles. The investigation of the above mentioned phenomena can be used to obtain additional information on the dynamics of the vortex lattice,³⁰ the periodicity of the underlying potential, and the density of particles in the system.³¹ In other words, high-frequency experiments provide further insight into the microscopic motion of vortices not available with the averaged response presented in Secs. IV–VI.

The synchronous motion of vortices resulting from the resonant condition $f=v/d$, known as mode-locking effect, allows one to obtain the exact number of v-av pairs created by the magnetic template. Indeed, the value of the average velocity is given by

$$v = cfd, \quad (2)$$

with d as the periodicity of the lattice in the direction of motion, f as the frequency of the rf current, and c as the

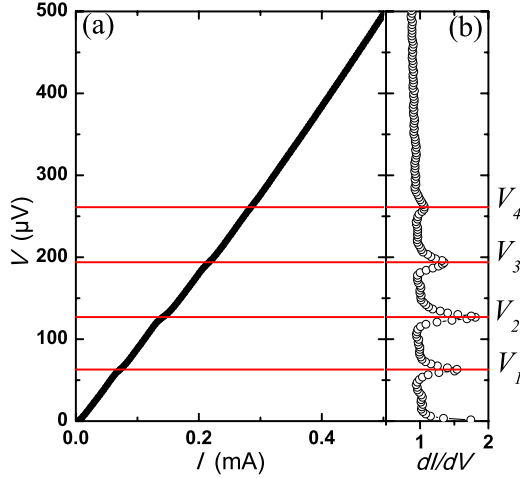


FIG. 7. (Color online) (a) $V(I)$ measurement (filled symbols) at $H=0.5$ mT and $T=1.1$ K with a small ac excitation of 100 MHz. Panel (b) shows a dI/dV , the discrete peaks are labeled according to Eq. (3).

number of cells that a vortex has traveled during a rf cycle. As we mentioned above, the fingerprint of this type of resonant motion is the presence of clear plateaus in the $I(V)$ characteristics separated by voltage steps,

$$V_c = Nk \frac{h v}{2e d} = Nk \frac{h}{2e} c f, \quad (3)$$

with k the number of vortices in each unit cell and N the number of rows between two voltage contacts. Measuring the voltage separation between consecutive steps and using Eq. (3) we can estimate the density of vortices moving coherently in the flux-flow regime.

Figure 7(a) shows a $V(I)$ scan for $H=0.5$ mT and $T=1.1$ K with a small ac excitation $I_{\text{rf}} \ll I_{\text{dc}}$ of 100 MHz superimposed.³² The presence of Shapiro steps in the linear part of the $V(I)$ curve becomes more apparent by plotting V versus dI/dV [see Fig. 7(b)]. These steps represent a clear indication of the coherent flow of vortices.

In Fig. 7(b) we assign the present peaks to values of V_c with c ranging from 1 to 4 ($V_1=63$ μV , $V_2=127$ μV , $V_3=194$ μV and $V_4=261$ μV). From their linear dependence on c , shown in the inset of Fig. 8, we calculate a value of $k \approx 1.06$. An independent estimation can be obtained by tracking the frequency dependence of each voltage plateau V_c . This is shown in Fig. 8 for the first two steps. The linear fit using Eq. (3) gives $k \approx 1.1$ and 1.18 for V_1 and V_2 , respectively.

It is important to notice that, in general, two ingredients are necessary for the presence of mode-locking effects. First, the existence of a flux-flow regime, which ensures a narrow distribution of average vortex velocities.³³ Second, there should be a periodic perturbation of the pinning potential, otherwise the distortion of the vortex lattice becomes too strong and its coherent motion is destroyed. In principle, this second condition is only fulfilled at the matching field, H_1 . This seems to be in contradiction with the fact that clear Shapiro steps are present at 0.5 mT, a field which would

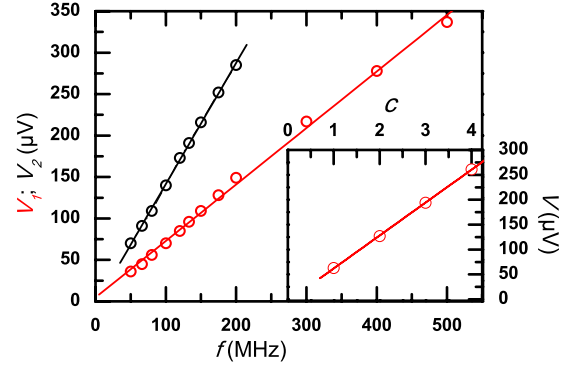


FIG. 8. (Color online) Frequency dependence of V_1 (circular symbols) and V_2 (square symbols) at a field of 0.5 mT and temperature of 1.1 K. Inset: $V_1 \rightarrow V_4$ measured at 100 MHz.

corresponds to 0.42 vortices per unit cell. This apparent paradox can be solved invoking once again the presence of v-av pairs induced by the triangles. In this case, the applied field will annihilate the vortices in the channel with opposite polarity, leading to an increase in their critical current and consequently suppressing their contribution to the coherent motion. On the other hand, the row with equal polarity will be unaltered by the applied magnetic field and therefore should exhibit a region of field independent Shapiro steps. In other words, the incoming vortices generated by the external magnetic field play no role in the coherent oscillatory motion of vortices thus giving rise to a constant voltage separation between two consecutive Shapiro steps.

In order to check these hypotheses of self-organized commensurability we measured the field dependence of the Shapiro steps, which are better visualized as a peak in the dI/dV as previously shown in Fig. 7(b). The results of these measurements for $T=1.1$ K are summarized in Fig. 9 as a contour plot in the field-voltage plane, with maximum intensity representing the exact location of the V_c peaks. For magnetic field values ranging from $-H_1$ to $+H_1$ a clear field independence peak position is observed. This result confirms that the amount of particles, moving coherently, is independent of the applied external field.

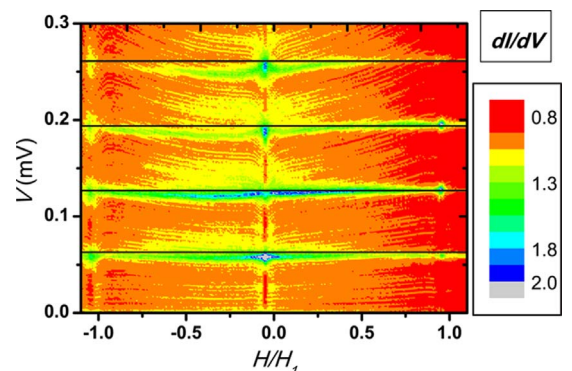


FIG. 9. (Color online) Magnetic field dependence of dI/dV versus V at a temperature of 1.1 K and an applied rf frequency of 100 MHz.

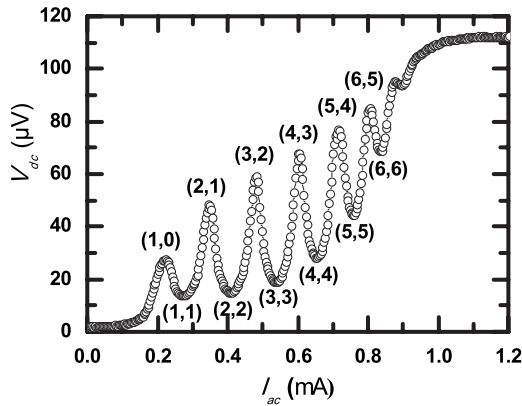


FIG. 10. dc voltage as a function of ac amplitude ($f = 100$ MHz) with a dc offset of $10 \mu\text{A}$ applied. The indexing (a, b) indicates the number of steps (a) forward and (b) backward.

VIII. DISCRETE MOTION OF THE VORTEX-ANTIVORTEX LATTICE

It has been predicted by molecular-dynamics simulations that a vortex lattice in a periodic landscape of asymmetric pinning sites can unveil the discrete hopping of vortices when the system is excited with a zero mean rf drive.^{34–36} So far, most of the experimental reports evidence a vortex rectification effect obtained in the low frequencies limit which results from an averaging in time and are not able to resolve the individual motion.^{37,38} In this section, we will try to bridge this gap by constructing an artificial vortex rectifier resulting from a dc tilt, which breaks the inversion symmetry of our system.³⁹ Additionally, this tilt allows us to probe the discrete motion of the vortex lattice without the need of a time resolved signal read out.

Figure 10 shows the dc voltage as a function of the applied ac drive with an additional dc on top ($I_{dc} = 10 \mu\text{A}$). Due to the applied dc tilt the critical current, needed to depin vortices, is smaller for positive than for negative currents ($I_{pos} < I_{neg}$). Depending on the strength of the applied ac amplitude I_{ac} we can determine three different dynamic regimes. For small ac excitations ($I_{ac} < I_{pos} < I_{neg}$) the driving force is unable to depin the vortices and as a result the dc voltage is zero. By increasing the ac amplitude above I_{pos} the vortex lattice is set in the flux-flow regime and mode-locking effects result in an oscillatory dependence of the dc voltage as a function of the ac amplitude. Finally at high ac amplitudes the normal state is reached and $V_{dc} = R_n I_{dc}$. Each maxima and minima in dc voltage can be attributed to the discrete motion of the vortex lattice in the positive and negative cycle of the driving amplitude. To identify the motion, we introduce the indexing (a, b) in Fig. 10, with a and b the number of steps in the positive and negative direction, respectively. At I_{ac} , just above I_{pos} , the driving force is strong enough to move the vortex lattice one unit cell in the positive direction while no motion occurs in the negative cycle of the ac drive and a maximum in the dc voltage output occurs. If the ac amplitude passes I_{neg} a single back and forth step of the vortex lattice occurs and as such a strong reduction in the dc voltage is measured. This difference between back and forth motion of the vortex lattice, due to a small dc tilt, results in a dis-

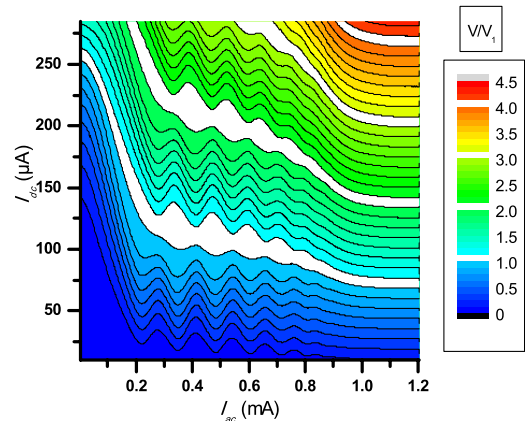


FIG. 11. (Color online) I_{ac} and I_{dc} dependence of the dc voltage at a magnetic field value of 1.195 mT and a rf modulation of 150 MHz.

crete stepping procedure up to the sixth order.

Figure 11 shows the dependence of the dc voltage, normalized to V_1 , as a function of the ac drive and the dc tilt. At small dc tilts (below $\approx 100 \mu\text{A}$) the behavior is exactly the same as shown in Fig. 10. In this region, the applied dc creates a small asymmetry and the vortex lattice, depending on the exact value of the ac drive, can either move one step extra in the positive direction (maxima in dc voltage) or an equal amount of steps in both directions (minima in dc voltage). Around $100 \mu\text{A}$ the oscillations vanish (white region) and the dc voltage readout amounts V_1 . The reason for this behavior is a subtle balance between the ac drive and the dc tilt. Exactly at the point where the ac amplitude is strong enough to move the vortex lattice in the “hard” direction (i.e., against the dc tilt) it is also sufficiently strong to move the vortex lattice an additional step in the “easy” direction. Therefore the overall motion of the vortex lattice will be independent on the applied ac drive and equal to 1. This subtle balance is destroyed in favor of easy flow if the applied dc is increased above $100 \mu\text{A}$. Again the dc voltage readout ($1 < V_{dc}/V_1 < 2$) indicates that the vortex lattice moves two steps (maxima in dc voltage) or one step (minima in dc voltage) extra in the positive direction. By increasing the dc tilt even further we could even see a difference of four unit cells between the motion in the positive and negative direction.

IX. CONCLUSION

We have demonstrated that the particular geometry of the twofold symmetric array of magnetic triangles can induce an order-disorder transition as the system switches from the as-grown state to the magnetized state. The disordered phase is characterized by a random distribution of two opposite chirality magnetic buckle states, whereas in the order state all triangles are in a well defined unique magnetic buckle state. The latter phase exhibits unidimensional lines of strong stray fields which represent channels for easy flux motion resulting in a clear anisotropy of the critical current. A quantitative estimation shows that the current needed to induce interchan-

nels hopping is about five times larger than that needed for setting intrachannel motion. It is important to stress that even though we have presented clear evidence of the influence of the ordering of magnetic dipoles induced by the magnetic templating on the vortex dynamics, it is still uncertain whether the ultimate source of disorder in the as-grown state is the random distribution of magnetic poles in the buckle state or the presence of triangles in the magnetic vortex state along one line of connecting triangles. In addition, we showed that the high mobility of the vortex lattice is a consequence of the generation of vortex-antivortex pairs by the magnetic template. This picture was confirmed experimentally by high-frequency transport measurements and low-frequency ratchet experiments. Due to the self-organized commensurability of these channels a pronounced mode-locking effect is observed. These features were used to probe

and tune the discrete motion of the composite lattice of vortices and antivortices. This combination of techniques represents a powerful tool for understanding the motion of vortices at microscopic scale.

ACKNOWLEDGMENTS

This work was supported by the K. U. Leuven Research Fund Program No. GOA/2004/02, NES–ESF program, the Belgian IAP, the Fund for Scientific Research–Flanders (F.W.O.–Vlaanderen). V.M. acknowledges funding support from U.S. NSF, Grant No. ECCS-0823813. A.V.S. and J.V.d.V. are grateful for the support from the F.W.O.–Vlaanderen. Finally the authors also would like to acknowledge the help of ScienTec and Nanotec with the MFM images.

-
- ¹A. V. Silhanek, W. Gillijns, V. V. Moshchalkov, V. Metlushko, and B. Ilic, *Appl. Phys. Lett.* **89**, 182505 (2006); N. Verellen, A. V. Silhanek, W. Gillijns, V. V. Moshchalkov, V. Metlushko, F. Gozzini, and B. Ilic, *ibid.* **93**, 022507 (2008); A. Hoffmann, L. Fumagalli, N. Jahedi, J. C. Sautner, J. E. Pearson, G. Mihajlovic, and V. Metlushko, *Phys. Rev. B* **77**, 060506 (2008); J. E. Villegas and K. D. Smith, Lei Huang, Yimei Zhu, R. Morales, I. K. Schuller, *ibid.* **77**, 134510 (2008); V. Vlasko-Vlasov, U. Welp, G. Karapetrov, V. Novosad, D. Rosenmann, M. Iavarone, A. Belkin, and W.-K. Kwok, *ibid.* **77**, 134518 (2008); A. Belkin, V. Novosad, M. Iavarone, J. Pearson, and G. Karapetrov, *ibid.* **77**, 180506(R) (2008).
- ²W. Gillijns, M. V. Milošević, A. V. Silhanek, V. V. Moshchalkov, and F. M. Peeters, *Phys. Rev. B* **76**, 184516 (2007).
- ³M. V. Milošević and F. M. Peeters, *Phys. Rev. B* **68**, 094510 (2003).
- ⁴I. F. Lyuksyutov and V. L. Pokrovsky, *Adv. Phys.* **54**, 67 (2005).
- ⁵D. G. Gheorghie, R. J. Wijngaarden, W. Gillijns, A. V. Silhanek, and V. V. Moshchalkov, *Phys. Rev. B* **77**, 054502 (2008); W. Gillijns, A. V. Silhanek, and V. V. Moshchalkov, *ibid.* **74**, 220509(R) (2006).
- ⁶M. V. Milošević and F. M. Peeters, *Phys. Rev. B* **69**, 104522 (2004).
- ⁷M. Lange, M. J. Van Bael, A. V. Silhanek, and V. V. Moshchalkov, *Phys. Rev. B* **72**, 052507 (2005).
- ⁸G. Carneiro, *Physica C* **432**, 206 (2005).
- ⁹C. C. de Souza Silva, A. V. Silhanek, J. Van de Vondel, W. Gillijns, V. Metlushko, B. Ilic, and V. V. Moshchalkov, *Phys. Rev. Lett.* **98**, 117005 (2007).
- ¹⁰A. V. Silhanek, W. Gillijns, V. V. Moshchalkov, V. Metlushko, F. Gozzini, B. Ilic, W. Uhlig, and J. Unguris, *Appl. Phys. Lett.* **90**, 182501 (2007).
- ¹¹See C. A. F. Vaz, C. Athanasiou, J. A. C. Bland, G. Rowlands, *Phys. Rev. B* **73**, 054411 (2006), and references therein.
- ¹²J. Militat and A. Thiaville, *Science* **298**, 555 (2002).
- ¹³D. K. Koltsov, R. P. Cowburn, and M. E. Welland, *J. Appl. Phys.* **88**, 5315 (2000); D. K. Koltsov and M. E. Welland, *ibid.* **94**, 3457 (2003).
- ¹⁴Micromagnetic simulation is performed by a publicly available code from NIST (<http://math.nist.gov/oommf>).
- ¹⁵Higher criteria exhibit similar results.
- ¹⁶M. Lange, M. J. Van Bael, and V. V. Moshchalkov, *Phys. Rev. B* **68**, 174522 (2003).
- ¹⁷E. Rosseel, T. Puig, M. Baert, M. J. Van Bael, V. V. Moshchalkov and Y. Bruynseraede, *Physica C* **282-287**, 1567 (1997).
- ¹⁸V. V. Moshchalkov, L. Gielen, C. Strunk, R. Jonckheere, X. Qiu, C. Van Haesendonck, and Y. Bruynseraede, *Nature (London)* **373**, 319 (1995).
- ¹⁹Typically the temperature resolution achieved in our experimental setup is about 100 μ K.
- ²⁰It is worth noticing that the same matching field is obtained by the pinning produced by the thickness modulation of the Al film evaporated on top of the Py structure. However, this sort of nonmagnetic pinning is independent of the magnetic state of the Py structures and has much weaker strength. The comparison between the pinning produced by thickness modulations with that induced by magnetic particles has been addressed in previous investigations by Y. Jaccard, J. I. Martin, M.-C. Cyrille, M. Velez, J. L. Vicent, and Ivan K. Schuller, *Phys. Rev. B* **58**, 8232 (1998); A. Hoffmann, P. Prieto, and I. K. Schuller, *ibid.* **61**, 6958 (2000).
- ²¹A. S. Mel'nikov, Yu. N. Nozdrin, I. D. Tokman, and P. P. Vyshelev, *Phys. Rev. B* **58**, 11672 (1998).
- ²²R. Laiho, E. Lahderanta, E. B. Sonin, and K. B. Traito, *Phys. Rev. B* **67**, 144522 (2003).
- ²³C. L. S. Lima and C. C. de Souza Silva, arXiv:0808.2421 (unpublished).
- ²⁴A much weaker rectification signal is observed when the Lorentz force is parallel to the v-av channels.
- ²⁵P. Martinoli, O. Daldini, C. Leemann, and E. Stocker, *Solid State Commun.* **17**, 205 (1975).
- ²⁶A. T. Fiory, *Phys. Rev. Lett.* **27**, 501 (1971).
- ²⁷O. Daldini, P. Martinoli, J. L. Olson, and G. Berner, *Phys. Rev. Lett.* **32**, 218 (1974).
- ²⁸L. Van Look, E. Rosseel, M. J. Van Bael, K. Temst, V. V. Moshchalkov, and Y. Bruynseraede, *Phys. Rev. B* **60**, R6998 (1999).
- ²⁹S. Shapiro, *Phys. Rev. Lett.* **11**, 80 (1963).
- ³⁰N. Kokubo, B. Shinozaki, and P. H. Kes, *Physica C* **468**, 581 (2008).

- ³¹N. Kokubo, R. Besseling, V. M. Vinokur, and P. H. Kes, Phys. Rev. Lett. **88**, 247004 (2002).
- ³²Since the ac excitation is applied by a function generator, it is necessary to calibrate the transmitted current, I_{rf} , as a function of the fed voltage. In order to estimate their value we have used both direct and indirect measurement techniques. For the latter we investigate the influence of the ac excitation on the $V(I_{\text{dc}})$ characteristics. For instance in the experiments presented in Sec. VII all used ac excitations introduce a very small perturbation and we can safely assume that $I_{\text{rf}} \ll I_{\text{dc}}$. In Sec. VIII the perturbation is stronger and we estimate the induced ac currents by measuring the shift in critical current ($I_c = I_{\text{ac}} + I_{\text{dc}}$) as a function of the applied ac drive.
- ³³P. Martinoli, O. Daldini, C. Leemann, and B. Van den Brandt, Phys. Rev. Lett. **36**, 382 (1976).
- ³⁴C.-S. Lee, B. Jankó, I. Derényi, and A.-L. Barabási, Nature (London) **400**, 337 (1999).
- ³⁵B. Y. Zhu, F. Marchesoni, V. V. Moshchalkov, and Franco Nori, Phys. Rev. B **68**, 014514 (2003).
- ³⁶Q. Lu, C. J. Olson Reichhardt, and C. Reichhardt, Phys. Rev. B **75**, 054502 (2007).
- ³⁷J. E. Villegas, Sergey Savel'ev, Franco Nori, E. M. Gonzalez, J. V. Anguita, R. García, and J. L. Vicent, Science **302**, 1188 (2003).
- ³⁸J. Van de Vondel, C. C. de Souza Silva, B. Y. Zhu, M. Morelle, and V. V. Moshchalkov, Phys. Rev. Lett. **94**, 057003 (2005).
- ³⁹C. C. de Souza Silva, J. Van de Vondel, B. Y. Zhu, M. Morelle, and V. V. Moshchalkov, Phys. Rev. B **73**, 014507 (2006).